Heterogeneity of layer 4 in visual areas of rhesus macaque cortex

Dorothee M. Günther[1,2,5]†, Mykhailo Y. Batiuk[3,4]†, Viktor Petukhov[3], Romain De Oliveira[3], Thomas Wunderle[1], Christian J. Buchholz[5], Pascal Fries[1,2]‡, Konstantin Khodosevich[3]‡§

[1]Ernst Strüngmann Institute (ESI) for Neuroscience in Cooperation with Max Planck Society, 60528 Frankfurt, Germany
[2]Donders Institute for Brain, Cognition and Behaviour, Radboud University Nijmegen, 6525 EN Nijmegen, the Netherlands
[3]Biotech Research and Innovation Centre (BRIC), Faculty of Health and Medical Sciences, University of Copenhagen, 2200 Copenhagen, Denmark.
[4]Brain Mind Institute, School of Life Sciences, École Polytechnique Fédérale de Lausanne (EPFL), CH-1015 Lausanne, Switzerland.
[5]Molecular Biotechnology and Gene Therapy, Paul-Ehrlich-Institut, 63225 Langen, Germany

†These authors contributed equally to this work.
‡ These authors contributed equally to this work.
§Correspondence should be addressed to konstantin.khodosevich@bric.ku.dk

Abstract

Recently, single-cell RNA-sequencing (scRNA-seq) has enabled unprecedented insights to the cellular landscape of the brains of many different species, among them the rhesus macaque as a key animal model. Building on previous, broader surveys of the macaque brain, we closely examined five immediately neighboring areas within the visual cortex of the rhesus macaque: V1, V2, V4, MT and TEO.

To facilitate this, we first devised a novel pipeline for brain spatial archive – the BrainSPACE – which enabled robust archiving and sampling from the whole unfixed brain. SnRNA-sequencing of ~100,000 nuclei from visual areas V1 and V4 revealed conservation within the GABAergic neuron subtypes, while seven and one distinct principle neuron subtypes were detected in V1 and V4, respectively, all most likely located in layer 4. Moreover, using small molecule fluorescence in situ hybridization, we identified cell type density gradients across V1, V2, V4, MT, and TEO appearing to reflect the visual hierarchy. These findings demonstrate an association between the clear areal specializations among neighboring areas with the hierarchical levels within the visual cortex of the rhesus macaque.

Introduction

Human-related animal models such as non-human primates (NHP) play a crucial role in deciphering human brain physiology and diseases. Among the NHP family, the rhesus macaque is one of the most studied models that has been especially fruitful for understanding information processing in human visual cortex.

Studies in rhesus macaques identified intricate specialization of the visual cortex into several distinct areas. Those include primary visual cortex (V1) and V4, which together likely constitute the most studied primate brain areas with V4 serving as a core model for higher visual areas. V1 locates at the bottom of the hierarchy of visual areas and represents the cortical input area for processing of visual information [1-3]. From V1, information is sent to hierarchically higher areas that are organized into two distinct streams of visual information processing. Those are the ventral stream, in which information is passed from V1 to V2, V4, area inferior temporal area (TEO) [4] and further, to subserve object recognition, and the dorsal stream that includes the middle temporal area (MT) as a core higher visual area and is involved in motion and object location representation [5].

Visual information from the thalamus enters V1 through the granular cortical layer, layer 4. After local processing, V1 sends information to higher areas including V4 using feedforward projections that largely originate in the supragranular layers, layers 2 and 3 [6] and target layer 4 of V4 [3]. Information is also transferred backwards from V4 to V1 using feedback projections that originate primarily in the infragranular layers, layers 5 and 6 [6], of V4 and terminate outside of layer 4 in V1 [3]. Thus, V1 and V4 differ in cortical layers that receive and send signals, as well as sources and types of information that is received, processed, and transferred. However, how do such differences relate to structural and molecular correlates?

Classically, cortical areas have been defined based on their anatomy and cellular composition, for instance the number and widths of layers, neuronal morphology and composition, and intra- and interareal connectivity. Importantly, implementation of high-resolution single-cell and spatial transcriptomics in recent years revolutionized our understanding of neuronal diversity in cortical functional areas and pointed to a relation between this diversity and specific cortical functions [7-12]. In the rhesus macaque brain, single-cell and spatial transcriptomics allowed to generate atlases that revealed the high-resolution cytoarchitecture of cortical areas [13]. While these atlases provide deep insights into the cortical structure in rhesus macaque and its relation to mouse, human and other primates, there is a relative lack of single-cell transcriptomics studies focused on neighboring yet specialized rhesus-macaque visual cortex areas, which are essential to understand structure-function relationships in visual information processing.

Here, we provide a single-cell transcriptomics atlas for early and mid-level visual cortex in the rhesus macaque. We first devised a novel brain-tissue banking pipeline for fast and precise sampling, storage and retrieval of rhesus-macaque brain tissue. We implemented the pipeline to identify five areas involved in visual processing, specifically areas V1, V2, V4, MT, and TEO. V1 and V4 were analyzed with snRNA-seq, and all five areas were further analyzed by snRNA-seq-informed multiplexed single-molecule florescent in situ hybridization (smFISH). Our snRNA-seq analysis of V1 and V4 revealed high conservation within GABAergic neurons, whereas there was a strong area-specific signature for all principal neuron subtypes. Moreover, seven distinct transcriptomic subtypes were detected specifically among principal neurons of V1, all most likely from layer 4, and one subtype specifically among principal neurons of V4 area. Follow-up smFISH analysis for several of these specific subtypes demonstrated transcriptional gradients across V1, V2, V4, MT, and TEO, which appear to largely reflect the functional hierarchy of these areas. Overall, our data show an association between the hierarchical levels and corresponding functions of the investigated areas to their unique organization. Further exploration of our atlas by the community is streamlined by an interactive online platform showing the V1 dataset (http://kkh.bric.ku.dk/p2auto/index.html?fileURL=http:/rdo/project_1/visualisation_2.bin), the V4 dataset (http://kkh.bric.ku.dk/p2auto/index.html?fileURL=http:/rdo/project_1/visualisation_3.bin) and the integrated data set (http://kkh.bric.ku.dk/p2auto/index.html?fileURL=http:/rdo/project_1/visualisation_1.bin).

Results

Novel pipeline for brain-tissue banking for storage and multi-purpose use

The rhesus macaque cortex is comprised of roughly 140 anatomically defined areas [14], and within the visual cortex, 29 areas are distinguished, among them V1, V2, V4, MT, and TEO (Fig. 1A). To enable precise and systematic sampling from banked brain material for follow-up analyses, such as snRNA-seq, we designed a box for dissection and storage, the BrainSPACE (Brain SPatial ArChivE). Within 30 minutes of the onset of cardiac arrest (see Methods for details), the skull was opened (Fig. 1B), and the whole brain was extracted and transferred to ice-cold buffer to reduce the degradation of RNA and proteins in the freshly dissected tissue. We removed the cerebellum and separated the hemispheres along the midline, to be able to position each hemisphere with its relatively flat medial surface on the precooled spacer plate (Fig. 1C). The hemisphere froze onto the spacer plate, attaching the tissue in place and allowing a cut along the spacers into a 2 mm thick sagittal section. Then the rest of the hemisphere was placed, with the freshly cut surface

down, onto the next spacer plate and the process was repeated until the whole hemisphere was cut into eight to nine 2 mm thick sagittal sections. All sections were imaged on the spacer plate before storing the spacer plates in the BrainSPACE box at -80°C (Fig. 1B) for further use. Using the images for manual alignment to an atlas [15], areas were identified and sampled from the respective slices. From the frozen slices, 5-10x10 mm blocks from the respective areas spanning all cortical layers and including white matter were extracted from V1, V2, V4, MT and TEO (Fig. 1 C- D).

Taxonomy of neuronal types across visual areas

Tissue samples from areas V1 and V4 from rhesus macaques P and A were collected and analyzed by single nucleus RNA-sequencing (snRNA-seq) in this study. To this end, 5x10 mm tissue blocks were homogenized, and neuronal nuclei were sorted by fluorescent-activated nuclear sorting (FANS) using an antibody to a general neuronal marker NeuN (Supplement Fig. 1A) as described before [16]. SnRNA-seq was performed using the 10X Genomics protocol. In total, we sequenced 95,071 neuronal nuclei from 2 rhesus macaques (1 male, 1 female), 53,144 from V1 and 41,927 from V4 (4182 median Unique Molecular Identifiers (UMIs) and 2164 median genes per nucleus) (Supplement Fig. 1B-D). In order to annotate the neuronal populations consistently, inter-individual variations were minimized by aligning the samples from V1 and V4. The subpopulations were hierarchically annotated across all samples. First, at the lowest resolution, principal neurons and GABAergic neurons were separated. Further separation of major families of principal and GABAergic neurons was done using family-specific marker genes for principal neurons (*CUX2*, *RORB*, *FEZF2*, *THEMIS*) and for GABAergic neurons (*ID2*, *PVALB*, *SST*, *VIP*) (Fig. 2 DE). Next, for each family, we identified fine-resolution transcriptomic subtypes, which in some cases could be grouped in subfamilies based on common markers and similarities present in several subtypes (for instance, L5_FEZF2_PDYN and L5/6_FEZF2_TLE4) (Fig. 2DE). To name subfamily and subtype, we chose among the most specific markers labeling a corresponding cluster, where subtypes with subfamily category had three hierarchical gene markers (family_subfamily_subtype), and those without subfamily category had two hierarchical gene markers (family_subtype). At highest resolution, we could distinguish 46 transcriptomic subtypes, 23 of which belonged to principal neurons and 23 of them to GABAergic neurons (Fig. 2B, Supplement Fig. 2).

To identify potential impact of covariates, such as individual, sex, hemisphere, kit version and sequencing batch, on subtype annotation, we labeled each of these major covariates and showed that they were evenly distributed across UMAPs (Supplement Fig. 3A-F).

Comparative analysis reveals strong areal differences of neuronal complexity in the visual cortex

Integration of V1 and V4 data revealed general principles for areal specialization in the visual cortex. While GABAergic neuron subtypes exhibited well-preserved conservation of expression patterns, principal neurons showed strong areal differences (Fig. 2C). Although generally similar patterns have been reported for the regional patterning of mouse and human cortex, for instance primary motor (M1) vs primary visual (V1) cortical areas [11, 17], here we show that cortical area patterning might have some unique features.

Most striking was the finding of general strong differences between principal neuron subtypes of V1 vs V4. Principal neuronal subtypes revealed different areal expression signatures as well as completely unique subtypes in both areas (Fig. 3A, Supplement Fig. 4A). All unique subtypes of principal neurons were concentrated in layer 4 (L4) (Fig. 3BC, Supplement Fig. 4B), with 7 unique subtypes in V1 (L4_RORB_KCNH8_SEMA5A, L4_RORB_KCNH8_ARHGAP24, L4_RORB_KCNH8_KCNB2, L4_RORB_KCNH8_PARD3, L4_RORB_KCNH8_SPOCK3, L4_RORB_MET_CRISPLD1 and L4_RORB_MET_KCNIP1) and 1 unique subtype in V4 (L4_RORB_KCNH8_ABCA12). Interestingly, most unique L4 subtypes were of the RORB_KCNH8 subfamily (Fig. 3A), which might be a unique subfamily for the visual cortex in rhesus macaque, since strong *KCNH8* gene expression enrichment in the macaque visual vs prefrontal and motor cortices has been reported before [18].

We also noticed a general shift in principal neuron/GABAergic neuron ratio in V1 compared to V4. V4 had a larger fraction of GABAergic neurons than V1. Overall ratios of principal neuron/GABAergic neuron (P:G ratio) were 6.46 and 2.75 for V1 and V4, respectively (Fig. 3D). Additionally, when we measured compositional changes for all common subtypes in V1 and V4, we found most significant increases in principal neuron subtypes in V1 (mainly in L4-6 subtypes) (Fig. 3E). It was opposite for V4, where increases in GABAergic neuron subtypes were the most significant, with VIP neuron subtypes exhibiting the largest enrichment (Fig. 3E). This indicates potential differences in excitation/inhibition ratios in V1 and V4.

To explore pathways that might shine light on the function of the unique cell types in V1 and V4, we extracted the top up- and down-regulated genes for each cell type and calculated the enriched GeneOntology (GO) terms. Analysis for up-regulated enriched GO terms in cell subtypes in V1 and V4 revealed major clustering of GO terms (Fig. 4A). The top 3 GO terms per cell type were all related to cell adhesion and neuron development. Interestingly, the cell type L4_RORB_ABCA12 (only found in V4) also showed enriched GO terms related to cell adhesion and neuron development. The other cell types found in layer 4 of V1 and V4, although also belonging to the family of *RORB,* did not show

enrichment in these groups of GO terms (Fig. 4A). Analysis of the genes associated with the enriched GO terms showed frequent occurrence of the genes *NTNG1*, *NLGN1* and *SPOCK1*. While *NTNG1* and *NLGN1* appear to be highly expressed in the same cell types in V1, *SPOCK1* is highly expressed in L4_RORB_KCNH8_ABCA12 (V4 specific) and L4_RORB_KCNH8_ARHGAP24 (Fig 4B). *NTNG1* is known for its role in neurite outgrowth [19] and is associated with the Rett syndrome [20] and schizophrenia [21]. *NLGN1* and *SPOCK1* are associated with synapse formation [22, 23], and *NLGN1* is associated with autism [24]. Analysis for down-regulated enrichment did not show a similarly clear picture, revealing only slight enrichment of GO terms related to muscle contraction (Supplement Fig. 5D).

Gradient principle of L4 neuronal subtypes distribution in the areas of the visual cortex

To reveal general principles of distribution of V1/V4-unique subtypes of L4 principal neurons across visual cortex areas, we first identified most suitable markers for smFISH of 4 unique populations using the conos package (Fig. 3B). For the populations V1 L4_RORB_KCNH8_PARD3 and L4_RORB_MET_CRISPLD1, the respective subtype markers (*PARD3* and *CRISPLD1*) were chosen, for V1 L4_RORB_KCNH8_SPOCK3, the marker *ZNF385D*, and for L4_RORB_MET_KCNIP1, the marker *PDE1A* were identified as suitable markers for smFISH analysis.

The focus was set on the layer 4 excitatory neuronal subtypes, and two subtypes from each subfamily L4_RORB_KCNH8 and L4_RORB_MET were selected. To expand the picture of compositional change in the visual cortex, more areas along the visual hierarchy were included, namely V1, V2, V4, MT and TEO. We labelled the Calcium/Calmodulin-Dependent Protein Kinase II Alpha (*CAMK2A*) as a common marker for excitatory neurons along with the RAR Related Orphan Receptor B (*RORB*) that was determined in snRNA-seq to be the family marker for layer 4 and layer 5 excitatory neurons. The third marker was chosen to determine the selected subtypes.

Multi-colour smFISH as well as Nissl staining was performed (Fig. 5A). Layers were identified based on the density of nuclei (DAPI), Nissl stainig, *CAMK2A* and the strong expression of *RORB* (Fig. 5B).

Quantification of the different markers for all tested areas revealed an interindividual variation and therefore increased variance between the individual data points reaching from percentages of about 1.5% to 40% of positive cells. For single replicates, positivity could reach up to 65% (Fig 6 A-D).

Three out of four subtypes showed significantly higher occurrence of the respective cell type in area V1 than in area V4 (L4_RORB_KCNH8_PARD3 (*PARD3*), L4_RORB_MET_CRISPLD1 (*CRISPLD1*) and L4_RORB_KCNH8_SPOCK3 (*ZNF385D*)), in line with the results from snRNA-seq (Fig 6 B-E) and confirming in general the snRNA-seq findings.

In accordance with the high specialization of layer 4 in V1, these cell types seem to decrease in abundance for hierarchically higher areas like V4 an MT, whereas TEO does not show a further decrease in subtype density but rather an increase.

Cell type L4_RORB_MET_KCNIP1 (*PDE1A*) shows a completely different picture. Instead of decreasing cell density towards higher areas, there seems to be an increase from V1 to V4 and MT and further to TEO. V2 shows an extraordinarily high density of the subtype with mean positivity of up to approx. 35%.

To validate the layer annotation, quantification of subtypes in layers 2/3 and 5 was performed. The picture resembles the results from area-wise quantification. For three out of four cell types, the percentage of triple positive cells is highest for layer 4 in area V1 and decreases to neighboring layers 2/3 and 5 (L4_RORB_KCNH8_PARD3, L4_RORB_MET_CRISPLD1 and L4_RORB_KCNH8_SPOCK3). For areas V2, V4, MT and TEO, the expression seems to be rather the lowest in layer 4, also confirming, that the chosen markers appear especially relevant for V1 layer 4.

Discussion

To understand the human visual system, the closely related rhesus macaque brain has proven to be one of the most valuable model systems. Indeed, our investigation of areas V1, V2, V4, MT and TEO revealed substantial complexity in their cell type compositions which corresponds with their hierarchical organization. Within the macaque visual cortex, V1 is likely the most studied area overall, and V4 is among the most studied higher visual areas, probably the most studied one in the ventral stream. Here, we sampled form V1 and V4 separately to investigate these areas in detail before directly comparing these two areas with regard to their gene expression patterns. Differences can be expected based on several lines of previous research. V1 and V4 differ anatomically. In fact, V1 is also referred to as striate cortex, because of the V1-specific stria of Gennari, a band of heavily myelinated axons between sublayers of its layer 4. This band is so prominent that in human visual cortex, it is visible even in the unfixed brain and to the naked eye. Correspondingly, substantial research has been devoted to V1 layer 4 and has described several sublayers with differential afferent and efferent projection patterns [25]. Besides the connection pattern, V1 layer 4 is also morphologically distinct in that it contains a large proportion of

spiny stellate cells [26]. All these features that are distinct for V1 layer 4 are likely related to its function of being the predominant target of visual input via projections from the LGN to the cortex.

Here we devised a method to effectively prepare and store unfixed macaque brain tissue for multiple downstream analysis methods. To identify principles of visual cortex area organization, we sampled ~100,000 neurons for snRNA-seq from areas V1 and V4. We were able to identify 23 GABAergic and 23 principal neuron types and to assign the principal neurons to the layers of the cortex according to their markers.

The first key finding in this study is that the GABAergic cell types are well conserved between areas V1 and V4, in line with studies from multiple other primates [8, 17, 27-29]. PVALB+ GABAergic neurons have been reported to be enriched in the occipital lobe of marmosets [29, 30], macaques [28] and humans [11]. In human, an SST+ GABAgergic subtype was uniquely found in V1, in line with findings by Chen et al [28] who report a group of SST+ interneurons that predominantly populates the occipital and parietal cortices in the macaque. We sampled from two areas within the occipital lobe and found GABAergic neuron types to be essentially identical.

The second key finding presents strong area specificities in principal neurons. Other studies in mouse and primates [11, 28, 29, 31] have shown that cell subtypes appear to be present in all cortical regions albeit in different proportion. Jorstad et al. (2023) additionally showed strong area signatures in human when comparing different regions. Remarkably, we can confirm the strong area signatures in our comparison of areas that are immediately neighboring in the occipital region. Confirming results from human and macaque snRNA-seq studies, we could identify an elevated principal neuron to GABAergic neuron ratio in V1 over V4 [11, 28].

The third key finding reveals 7 cell types, putatively from layer 4, being unique to V1 even when compared intra-regional to the closely related area V4, emphasizing the special role of V1 layer 4 [26]. V1 specific subtypes in layer 4 were also reported in marmosets, macaques and humans [8, 28, 29]. All 7 cell types showed a strong expression of the family marker RORB which has been detected in V1 layer 4 principal neuron subtypes in the cynomolgus macaque [28] and marmoset [29] V1 as well as in primary areas of other systems (e.g. somatosensory system [32]). Additionally, 5 out of 7 subtypes showed strong expression of KCNH8, a marker combination that has been found in layer 4 in the visual system of marmosets [29]. GO term analysis revealed association with the gene NTNG1 as has also been shown by Chen et al [28]. The snRNA-seq datasets are freely accessible in the web tools for V1 and V4 separately as well as for an integrated dataset and will be a valuable resource for further comparative analysis. Additionally, the web tool allows easy

access to e.g. differentially expressed genes and might therefore also be a valuable resource for the development of cell-subtype specific targeting.

We used quantitative smFISH to validate and extend on the snRNA-seq findings, including three more areas, V2, MT and TEO, along the ventral and dorsal stream. The fourth key finding demonstrates a trend upon inclusion of V2 and MT, showing a decrease in cell type density moving along the dorsal stream to higher hierarchical areas for three out of four cell types (L4_RORB_MET_CRISPLD1, L4_RORB_KCNH8_SPOCK3 (ZNF385D) and L4_RORB_KCNH8_PARD3). This resembles reports of gene expression and cell type density decreasing in a gradual manner along the rostral-caudal axis [11, 31, 33] and from low to higher hierarchical areas [28]. Interestingly, when moving along the ventral stream to higher hierarchical areas like TEO located in the temporal lobe, we only see a decrease in cell type density from V1 through V2 to V4, but no further decrease in TEO. The last key finding confirmed the primary localization in V1 layer 4 showing a decrease of these cell types in layer 2/3 as well as in layer 4. While PARD3, CRISPLD1 and ZNF385D are specific for the cell types L4_RORB_KCNH8_PARD3, L4_RORB_MET_CRISPLD1 and L4_RORB_KCNH8_SPOCK3 (ZNF385D) and show a decrease of cell type density along the hierarchy as well as in layer 2/3 and layer 5, PDE1A shows an increasing cell type density from V1 to V4, MT and TEO, with the exceptionally high density in V2 appearing like an outlier data point. Similarly, for PDE1A, the highest density of cells in laver 5 (Supplement Fig. 6A) has also been shown in bulk seq analysis in layer-dissected rhesus macaque tissue [34]. Absent from V4 in the snRNA-seq data, cells of the V1-specific types were detected in V4 layer 4 in smFISH, albeit at much lower frequency than in V1, also blending into neighboring layers 2/3 and 5. The primary reason for this discrepancy in observed cell type distribution is the difference in the number of markers used for cell classification in smFISH versus snRNA-seq: While smFISH allows for a high-resolution assessment of cell distribution in space, it relies on a limited set of markers – in this case three – for cell classification. SnRNA-seq, on the other hand, integrates information from a much larger cross-section of markers but does not offer spatial information. MERFISH [35] and recently developed spatial sequencing [28, 36] methods combine the advantages of both approaches and will all for an even more fine-grained analysis of the cellular composition of the visual cortex. Secondary reasons may include the fact that only nuclear RNAs were assessed in snRNA-seq compared to smFISH as well as the comparatively low sequencing depth achieved in the former.

The present dataset was collected from four monkeys, albeit each method was only performed on two of them. Enlarging the data set using all four monkeys for snRNA-seq and smFISH will help reduce the impact of the inter-individual variance that is especially observed in the smFISH dataset. Additionally, including more cell-type specific markers for

the spatial detection might refine the detected pattern and might allow for the detection of more cell types.

Recent single-cell atlases of rhesus macaque and other primate species have impressively shown the enormous potential of single-cell technologies to characterize the complexity of brain tissue. By investigating areas of the visual cortex of the rhesus macaque brain, we add otherwise missing knowledge on areal organization and resolve areal complexity for the visual cortex, which should help understanding visual information processing. A major future challenge will be performing structure-functional studies in the visual cortex for direct association of specific neuronal subtypes to their functional roles.

Materials and Methods

Rhesus macaque tissue preparation

Rhesus macaque handling and housing conditions were in accordance with the German law for the protection of animals and the “European Union’s Directive 2010/63/EU” and approved by the local government office (Regierungspräsidum Darmstadt).

Rhesus macaques E and S were euthanized due to medial indications at high age. Brains from rhesus macaques 223 and 354 were kindly provided by the veterinary department of the Paul-Ehrlich-Institut, after they had been euthanized for collecting hematopoietic organs for another study (Supplementary table 1).

Rhesus macaque brain tissue was obtained from 4 *Macaqua mulatta* in total, 2 females and 2 males. As soon as death was confirmed by the veterinarian, the spine was broken and the tongue removed by two incisions (Fig. 1B – blue line). The head was cut off and the skull was exposed by pulling the skin and muscles from posterior to anterior up to the frontal skull. A hand saw was used to carefully open the skull along the red lines indicated in Figure 1B. The calotte was removed using a spatula, and the brain was pulled out of the skull by gravity. Cranial nerves were cut, and the brain was washed in ice-cold saline. The cerebellum was removed by inserting a spatula from posterior in between the occipital lobe and the cerebellum moving it into anterior direction until the stem brain was separated. The hemispheres were separated along the midline using a Virchow brain knife. The BrainSPACE, made from stainless steel, box was precooled to - 80°C over night. Before cutting the brain, the spacer plates with 2 mm space bars on two of their edges were placed onto dry ice. For the process of cutting, a spacer plate was removed from the dry ice and handled at room temperature. The hemisphere was placed onto the pre-frozen spacer plate with the medial side facing the plate. We waited until the tissue was frozen to the spacer plate indicated by tissue color change. Before the frozen tissue part reached the limit of the space bar, the brain knife was used to cut along the spacers, resulting in 2 mm thick tissue sections. Each brain slice was imaged using a high-resolution digital camera. The plate

carrying the brain slice was placed on dry ice for complete freezing, and the remaining hemisphere was placed, with the freshly-cut surface down, onto the next pre-cooled plate. This sequence was repeated until one entire hemisphere was cut into slices, and then repeated for the second hemisphere. Plates were stored in the BrainSPACE box at - 80 °C. Each hemisphere resulted in eight to nine sections depending on the size of the animal's brain.

For in situ hybridization, images obtained from the sagittal slices were compared to the rhesus macaque brain atlas [15], and areas V1, V2, V4, MT and TEO were identified according to the macroscopic anatomic landmarks like sulci and gyri. At the desired locations, the 2 mm thick slices were further cut to obtain 10 X 10 mm tissue cubes, using a hot scalpel as depicted in Figure 1C. Blocs were embedded in Tissue Freezing Medium (Leica, 14020108926) and stored at -20°C until further processing.

Nuclei isolation

Nucleus isolation was done as described before with slight modifications [37]. Tissue was removed from the -80°C and transferred into a 1 ml Dounce homogenizer holding 1 ml of prechilled homogenization buffer (250 mM Sucrose, 25 mM KCl, 5 mM MgCl2, 10 mM Tris pH 8.0, 1 mM DTT, 1 x protease inhibitor (Roche, 11873580001), 0.4 U/ul RNAse inhibitor (Takara, 2313B), 0.2 U/ul SUPERase•In (Invitrogen, AM2696), 0.1 % Triton X-100). Tissue was treated with 5 strokes of the loose pestle, followed by 15 strokes of the tight pestle and then filtered through a 40 µm cell strainer. Nuclei were spun down at 1000 x g for 8 min at 4 °C. Supernatant was aspirated, homogenization buffer was added to a total volume of 250 µl and nuclei were resuspended. Nuclei suspension was mixed with 250 µl 50 % Iodixanol (60 % stock from STEMCELL Technologies, 7820), 1 x protease inhibitor (Roche, 11873580001), RNAse inhibitor (0.4 U/ul; Takara, 2313B), SUPERase•In (0.2 U/ul; Invitrogene, AM2696) and 1 mM DTT and layered on top of a 29 % Iadixanol solution (25 mM KCl, 5 mM MgCl2, 10 mM Tris pH 8.0, 29 % Iodixanol, 1 x protease inhibitor, 0.4 U/ul RNAse inhibitor, 0.2 U/ul Superasin, 1 mM DTT) into an ultracentrifugation tube on ice. Gradients were placed into a swing bucket rotor (Beckman Coulter, TLS 55) and centrifuged at ~14.000 x g max (~10900 x g average) for 22 min at 4 °C (Beckman Coulter, MAX-XP). After centrifugation, supernatant was removed, nuclei were resuspendend in BSA blocking buffer (1 x PBS, 0.5 % BSA, 1 mM DTT, 2.54 mM MgCl2, 0.2 U/ul RNAse inhibitor) and incubated for 15 min on ice. Before staining, splits were taken for the controls (isotype control, negative control, 7AAD only control, NeuN only control). To the sample and NeuN only control, the neuronal marker NeuN antibody was added (1 µg/µl, 1:16949, Millipore, MAB3777X). To the isotype control, the control antibody was added (0.2 µg/µl, 1:3390, STEMCELL Technologies, 60070AD). Antibodies were incubated for 10 min at

4 °C in the dark. After the incubation, 1 ml BSA blocking buffer was added and centrifuged at 1000 x g for 10 min at 4 °C in a swing bucket. Pellets were resuspended in 200 µl BSA blocking buffer and filtered through a 35 µm strainer. Samples were filled with BSA blocking buffer to a total volume of 500 µl, and 0.75 µl of 7AAD (1 mg/ml, Sigma) was added. FACS was performed using BD FACSAria III sorter using a 75 µm nozzle and controlled by BD FACSDiva 8.0.1 software. Single color controls were used for compensation. Nuclei were sorted based on the gating strategy depicted in Supp. Fig 2A. Nuclei were collected into 5 µl of BSA blocking buffer at 4 °C. Nuclei were directly processed for 10x library preparation.

10x library preparation and sequencing

Chromium Single Cell 3' Reagent kit v2 (10x Genomics, 120237) and v3 (10x Genomics, 1000075) were utilized for library preparation. The standard protocol was applied as described before [16, 37]. In brief, nuclei were counted under a brightfield microscope and mixed with the reverse transcription mix. Either v2 or v3 Gel Beads were added, and the mix was partitioned on Chromium Chips A (v2 kit, 10x Genomics, 120236), or Chips B (10x Genomics, 1000073) into GEMs using the Chromium Controller (10x Genomics, PN-120223), and reverse transcription was performed. Then, samples were frozen at -20 °C until further processing. cDNA was cleaned up, pre-amplified (12 PCR cycles), SPRIselect cleaned up and quantified before being frozen again at -20 °C. If possible, the same amount of cDNA was used for fragmentation, end-repair and A-tailing. The following process was performed: SPRIselect clean up, adapter ligation, SPRIselect clean up, sample index PCR using Chromium i7 sample indices (10-13 PCR cycles, depending on cDNA input quantity, 10x Genomics, PN-120262), SPRIselect clean up and quantification using the Qubit HS dsDNA Assay kit (Thermo Fisher Scientific, Q32854) on the Qubit Fluorometer and the High Sensitivity DNA Kit (Agilent, 5067-4626) on the Bioanalyzer. The amount of nuclei was estimated and the libraries pooled accordingly. Pools were again quantified and sequenced on the Illumina NextSeq500 using NextSeq500/550High Output Kit v2.5 (Illumina, 20024907). The sequencing protocol included 26 cycles for read 1, 8 cycles for i7 index and 98 cycles for read 2 for 10x v2 kit or 28 cycles for read 1, 8 cycles for i7 index and 91 cycles for read 2 for 10x v3 kit.

Single nuclei sequencing data analysis

Primary data analysis was performed using the 10X Genomics CellRanger toolkit (version 3.1.0; https://support.10xgenomics.com/single-cell-gene-expression/software/pipelines/latest/what-is-cell-ranger). The reference genome sequence and annotation used were from Release 98 of the rhesus macaque genome from Ensembl

(http://ftp.ensembl.org/pub/release-98/fasta/macaca_mulatta/dna/Macaca_mulatta.Mmul_10.dna.toplevel.fa.gz; http://ftp.ensembl.org/pub/release-98/gtf/macaca_mulatta/Macaca_mulatta.Mmul_10.98.gtf.gz). The annotation file was further filtered to generate a GTF file for creating a pre-mRNA reference, where "transcript" was renamed to "exon" and retained in the final GTF using the following command: ``awk 'BEGIN{FS="\t"; OFS="\t";} $3 == "transcript"{ $3="exon"; print;}' Macaca_mulatta.Mmul_10.98.gtf > Macaca_mulatta.Mmul_10.98_PRE_mRNA.gtf`. Subsequently, the reference genome was generated for subsequent analyses using "cellranger mkref."

The Illumina ".bcl" files generated were initially demultiplexed using the "cellranger mkfastq" pipeline. Subsequently, reads were mapped against the reference genome, and UMIs were counted using the "cellranger count" pipeline. Subtype markers were then identified using the Conos "getDifferentialGenes" function (version 1.5.1; [38]) and further analyzed by manually inspecting marker expression patterns over UMAP maps of subtypes.

Compositional data, **Differential expression and gene ontology analysis**

Compositional data analysis was performed using Cacoa package, similarly as before [37, 39]. Dimensionality reduction was achieved using the UMAP algorithm in the "conos" package (version 1.5.1; [38]), resulting in a joint UMAP integration of the filtered dataset. Differential expression (DE) analysis was conducted using the "estimateDEPerCellType" function from the "cacoa" package (version 0.4.0; [39]) to identify genes significantly up- or down-regulated across different cell types, with independent filtering applied to enhance analysis accuracy (option: "DESeq2 Wald test" from the "DESeq2" package version 1.42.0; [40]).

To gain insights into the biological processes, cellular components, and molecular functions associated with differentially expressed genes in each cell type, Gene Ontology (GO) term enrichment analysis was performed. The "clusterProfiler" software (version 4.10.0; [41]) facilitated this analysis by mapping gene lists to annotated terms in the Gene Ontology database (package for Macaque GO term db: org.Mmu.eg.db version 3.18.0; [42]). The adjusted p-value for the top 3 GO term per cell type were visualized.

In situ hybridization

In situ hybridization was performed according to the manufacturer's instructions as stated in the protocol for fresh-frozen tissue (ACD – RNAScope Multiplex Fluorescent Reagent Kit v2 ((Cat No. 323100)). In brief, 10 µm sections were cut, fixed at 4 °C for 30 min,

dehydrated and treated with Hydrogen Peroxidase and Protease IV. The following RNAScope probes for macaca mulatta (Mmu) were purchased: Mmu-CAMK2A-C1 (Cat No. 461731), Mmu-RORB-C2 (Cat No. 876301-C2), Mmu-PDE1A-C3 (Cat No. 898751-C3), Mmu- PARD3-C3 (Cat No. 898731-C3), Mmu- CRISPLD1-C3 (Cat No. 898741-C3) and Mmu- ZNF385D -C3 (Cat No. 898711-C3). The probes were hybridized at 40 °C for 2 h, and the signal was amplified. The probes were visualized using the Opal-520 (visualizing C1), Opal-570 (visualizing C2) and Opal-690 (visualizing C3) (Akoya Cat No. NEL810001KT).

Image analysis and quantification

Images spanning all layers of the cortex were acquired at the Microscopy Core Facility at Paul-Ehrlich-Institut, Langen, Germany, on a Leica SP8 confocal laser scanning microscope using the tiling mode. Image analysis was performed in QuPath using the Analysis Guidelines from ACD (MK 51-154) for Fluorescent RNAScope image analysis.

Cortical layers were determined with the help of DAPI staining, CAMK2A and RORB visualization. Every layer was split in 5 roughly equal parts and marked with rectangles. Analysis was performed per rectangle. In brief, nuclei were detected and outline was enlarged by 3 µm for assuming a cell. Within the cell, positive probes above a manually set threshold were detected and counted. Thresholds were set per channel. A cell was defined as positive when more than 3 probes were detected. The percentage was calculated as cells positive for CAMK2A and RORB and target over cells being positive for CAMK2A and RORB. Statistical testing was performed using the chi-square test, and correction for multiple comparisons used the Bonferroni method.

References

1. Markov, N.T., et al., *Cortical high-density counterstream architectures.* Science, 2013. **342**(6158): p. 1238406.
2. Markov, N.T., et al., *A weighted and directed interareal connectivity matrix for macaque cerebral cortex.* Cereb Cortex, 2014. **24**(1): p. 17-36.
3. Felleman, D.J. and D.C. Van Essen, *Distributed hierarchical processing in the primate cerebral cortex.* Cereb Cortex, 1991. **1**(1): p. 1-47.
4. Boussaoud, D., R. Desimone, and L.G. Ungerleider, *Visual topography of area TEO in the macaque.* J Comp Neurol, 1991. **306**(4): p. 554-75.
5. Goodale, M.A. and A.D. Milner, *Separate visual pathways for perception and action.* Trends Neurosci, 1992. **15**(1): p. 20-5.
6. Barone, P., et al., *Laminar distribution of neurons in extrastriate areas projecting to visual areas V1 and V4 correlates with the hierarchical rank and indicates the operation of a distance rule.* J Neurosci, 2000. **20**(9): p. 3263-81.
7. Langlieb, J., et al., *The molecular cytoarchitecture of the adult mouse brain.* Nature, 2023. **624**(7991): p. 333-342.
8. Jorstad, N.L., et al., *Comparative transcriptomics reveals human-specific cortical features.* Science, 2023. **382**(6667): p. eade9516.
9. Campagnola, L., et al., *Local connectivity and synaptic dynamics in mouse and human neocortex.* Science, 2022. **375**(6585): p. eabj5861.
10. Lee, B.R., et al., *Signature morphoelectric properties of diverse GABAergic interneurons in the human neocortex.* Science, 2023. **382**(6667): p. eadf6484.
11. Jorstad, N.L., et al., *Transcriptomic cytoarchitecture reveals principles of human neocortex organization.* Science, 2023. **382**(6667): p. eadf6812.
12. Siletti, K., et al., *Transcriptomic diversity of cell types across the adult human brain.* Science, 2023. **382**(6667): p. eadd7046.
13. Zemke, N.R., et al., *Conserved and divergent gene regulatory programs of the mammalian neocortex.* Nature, 2023. **624**(7991): p. 390-402.
14. Van Essen, D.C., et al., *Cortical parcellations of the macaque monkey analyzed on surface-based atlases.* Cereb Cortex, 2012. **22**(10): p. 2227-40.
15. Saleem, K.S.L., N.K., *A Combined MRI and Histology Atlas of the Rhesus Monkey Brain in Stereotaxic Coordinates*. 2012.
16. Pfisterer, U., et al., *Identification of epilepsy-associated neuronal subtypes and gene expression underlying epileptogenesis.* Nat Commun, 2020. **11**(1): p. 5038.
17. Tasic, B., et al., *Shared and distinct transcriptomic cell types across neocortical areas.* Nature, 2018. **563**(7729): p. 72-78.
18. Lei, Y., et al., *Spatially resolved gene regulatory and disease-related vulnerability map of the adult Macaque cortex.* Nat Commun, 2022. **13**(1): p. 6747.
19. Lin, J.C., et al., *The netrin-G1 ligand NGL-1 promotes the outgrowth of thalamocortical axons.* Nat Neurosci, 2003. **6**(12): p. 1270-6.
20. Nectoux, J., et al., *Netrin G1 mutations are an uncommon cause of atypical Rett syndrome with or without epilepsy.* Pediatr Neurol, 2007. **37**(4): p. 270-4.
21. Wilcox, J.A. and S. Quadri, *Replication of NTNG1 association in schizophrenia.* Psychiatr Genet, 2014. **24**(6): p. 266-8.
22. Bonnet, F., et al., *Structure and cellular distribution of mouse brain testican. Association with the postsynaptic area of hippocampus pyramidal cells.* J Biol Chem, 1996. **271**(8): p. 4373-80.
23. Jeong, J., et al., *PSD-95 binding dynamically regulates NLGN1 trafficking and function.* Proc Natl Acad Sci U S A, 2019. **116**(24): p. 12035-12044.

24. O'Roak, B.J., et al., *Multiplex targeted sequencing identifies recurrently mutated genes in autism spectrum disorders.* Science, 2012. **338**(6114): p. 1619-22.
25. Gattass, R., et al., *Cortical visual areas in monkeys: location, topography, connections, columns, plasticity and cortical dynamics.* Philos Trans R Soc Lond B Biol Sci, 2005. **360**(1456): p. 709-31.
26. Vanni, S., et al., *Anatomy and Physiology of Macaque Visual Cortical Areas V1, V2, and V5/MT: Bases for Biologically Realistic Models.* Cereb Cortex, 2020. **30**(6): p. 3483-3517.
27. Chiou, K.L., et al., *A single-cell multi-omic atlas spanning the adult rhesus macaque brain.* Sci Adv, 2023. **9**(41): p. eadh1914.
28. Chen, A., et al., *Single-cell spatial transcriptome reveals cell-type organization in the macaque cortex.* Cell, 2023. **186**(17): p. 3726-3743 e24.
29. Krienen, F.M., et al., *A marmoset brain cell census reveals regional specialization of cellular identities.* Sci Adv, 2023. **9**(41): p. eadk3986.
30. Krienen, F.M., et al., *Innovations present in the primate interneuron repertoire.* Nature, 2020. **586**(7828): p. 262-269.
31. Yao, Z., et al., *A taxonomy of transcriptomic cell types across the isocortex and hippocampal formation.* Cell, 2021. **184**(12): p. 3222-3241 e26.
32. Clark, E.A., et al., *Cortical RORbeta is required for layer 4 transcriptional identity and barrel integrity.* Elife, 2020. **9**.
33. Burt, J.B., et al., *Hierarchy of transcriptomic specialization across human cortex captured by structural neuroimaging topography.* Nat Neurosci, 2018. **21**(9): p. 1251-1259.
34. Bernard, A., et al., *Transcriptional architecture of the primate neocortex.* Neuron, 2012. **73**(6): p. 1083-99.
35. Chen, K.H., et al., *RNA imaging. Spatially resolved, highly multiplexed RNA profiling in single cells.* Science, 2015. **348**(6233): p. aaa6090.
36. Stahl, P.L., et al., *Visualization and analysis of gene expression in tissue sections by spatial transcriptomics.* Science, 2016. **353**(6294): p. 78-82.
37. Batiuk, M.Y., et al., *Upper cortical layer-driven network impairment in schizophrenia.* Sci Adv, 2022. **8**(41): p. eabn8367.
38. Barkas, N., et al., *Joint analysis of heterogeneous single-cell RNA-seq dataset collections.* Nat Methods, 2019. **16**(8): p. 695-698.
39. Petukhov, V., et al., *Case-control analysis of single-cell RNA-seq studies.* 2022: p. 2022.03.15.484475.
40. Love, M.I., W. Huber, and S. Anders, *Moderated estimation of fold change and dispersion for RNA-seq data with DESeq2.* Genome Biol, 2014. **15**(12): p. 550.
41. Yu, G., et al., *clusterProfiler: an R package for comparing biological themes among gene clusters.* OMICS, 2012. **16**(5): p. 284-7.
42. Carlson, M. *Genome wide annotation for Rhesus*. 2019; Available from: http://bioconductor.org/packages/org.Mmu.eg.db/.

Acknowledgments

The authors would like to acknowledge Julien Vezoli (INSERM) for his advice on layer segmentation. The authors would like to thank Roland Plesker (Paul-Ehrlich-Institut) for extracting and providing two macaque brains.

Funding:

P.F. was supported by:
the German Research Foundation (DFG, FR2557/1-1, FR2557/2-1, FR2557/5-1, FR2557/7-1),
the European Union (FP7-604102-HBP),
the National Institutes of Health (NIH, 1U54MH091657-WU-Minn-Consortium-HCP).

RDO is funded by the European Union's Horizon 2020 research and innovation programme under the Marie Sklodowska-Curie grant agreement No. 945322.

Author contributions:
Conceptualization: PF, KK
Methodology: DMG, MYB, VP, RDO, TW, PF
Investigation: DMG, MYB, VP,
Visualization: DMG, MYB, VP, RDO
Supervision: CJB, PF, KK
Writing—original draft: DMG, MYB, RDO, PF, KK
Writing—review & editing: DMG, MYB, VP, RDO, TW, CJB, PF, KK

Competing interests:
P.F. has a patent on thin-film electrodes and is a member of the Advisory Board of CorTec GmbH (Freiburg, Germany).
All other authors declare they have no competing interests.

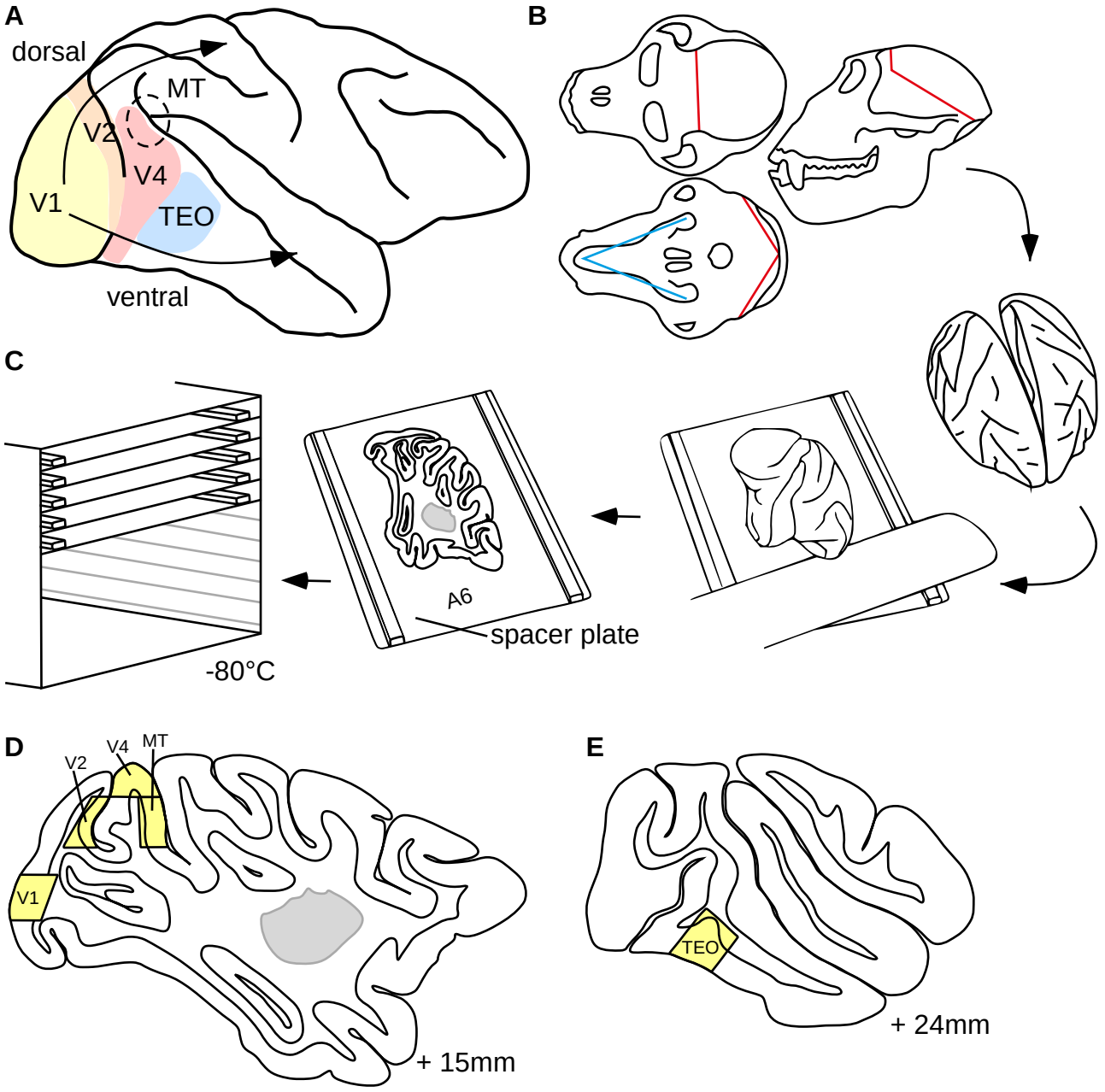

Fig. 1 Brain preparation and storage
(A) The rhesus macaque brain. Depicted are the primary visual area (V1), visual area 2 (V2), visual area 4 (V4), middle temporal area (MT) and area TEO including their location within the ventral and dorsal stream. **(B)** Drawings of the *macaca mulatta* skull from top (top left), bottom (bottom left) and side (right). Tissue cuts are marked in blue and bone saw cuts are marked in red. **(C)** Experimental design of the tissue sectioning. Hemispheres were separated, cerebellum removed and hemisphere placed with medial side onto cooled plate. Knife was moved along the bars (2 mm), rest of the hemisphere removed and placed onto the next plate. Plate was placed on dry ice until frozen and stored in box at -80°C. **(D)** 15 mm lateral section depicting the extracted tissue blocks for single cell sequencing and further treatment for smFISH. **(E)** 24 mm lateral section depicting the extracted tissue blocks for single cell sequencing and further treatment for smFISH.

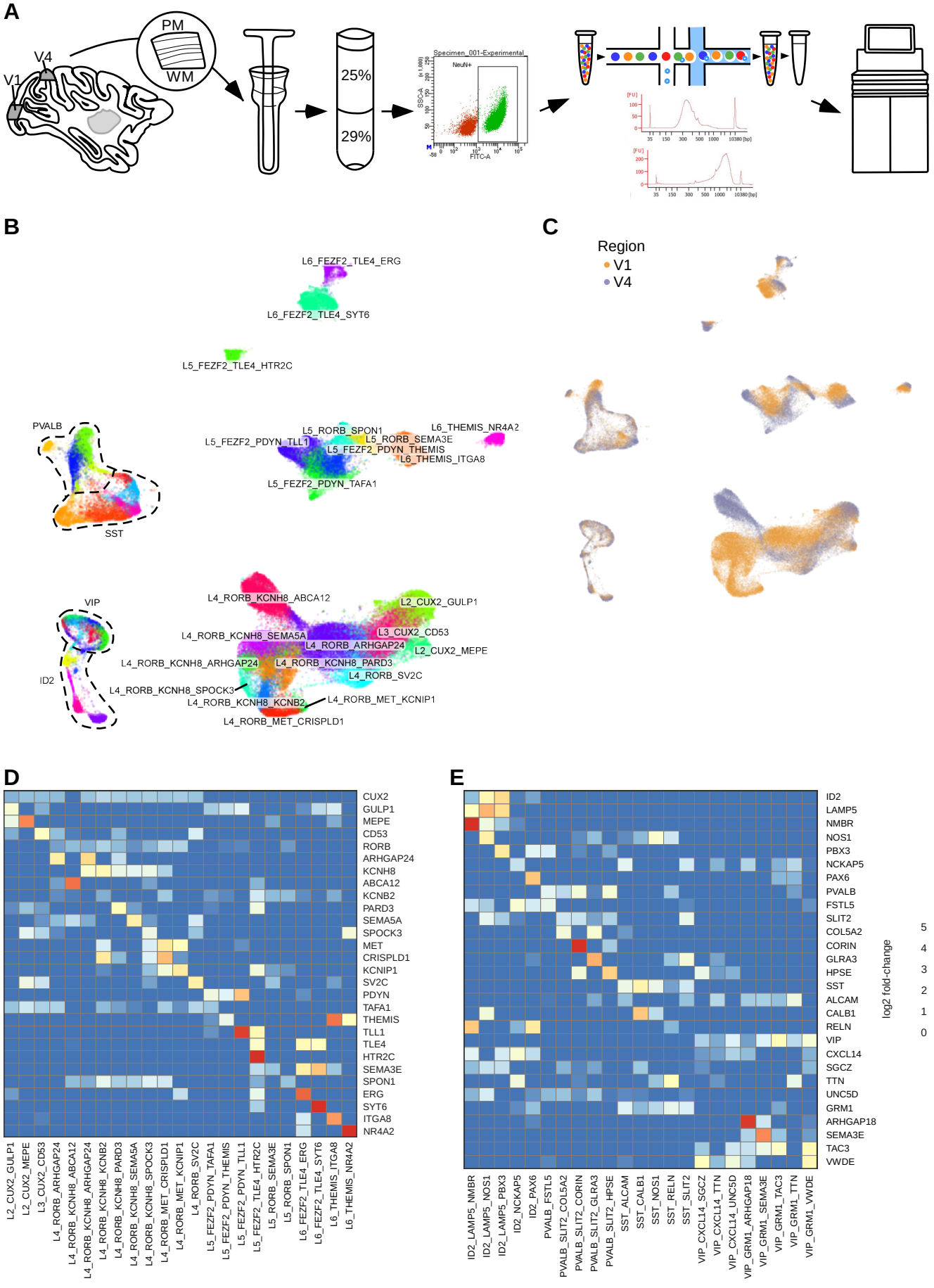
A
PM
WM
V4
V1
25%
29%
Specimen_001-Experimental
NeuN+
SSC-A
FITC-A
B
L6_FEZF2_TLE4_ERG
L6_FEZF2_TLE4_SYT6
L5_FEZF2_TLE4_HTR2C
PVALB
L5_RORB_SPON1
L6_THEMIS_NR4A2
L5_FEZF2_PDYN_TLL1
L5_RORB_SEMA3E
L5_FEZF2_PDYN_THEMIS
L6_THEMIS_ITGA8
L5_FEZF2_PDYN_TAFA1
SST
VIP
L4_RORB_KCNH8_ABCA12
L2_CUX2_GULP1
L4_RORB_KCNH8_SEMA5A
L3_CUX2_CD53
L4_RORB_ARHGAP24
L2_CUX2_MEPE
L4_RORB_KCNH8_ARHGAP24
L4_RORB_KCNH8_PARD3
L4_RORB_SV2C
ID2
L4_RORB_KCNH8_SPOCK3
L4_RORB_KCNH8_KCNB2
L4_RORB_MET_KCNIP1
L4_RORB_MET_CRISPLD1
C
Region
V1
V4
D
CUX2
GULP1
MEPE
CD53
RORB
ARHGAP24
KCNH8
ABCA12
KCNB2
PARD3
SEMA5A
SPOCK3
MET
CRISPLD1
KCNIP1
SV2C
PDYN
TAFA1
THEMIS
TLL1
TLE4
HTR2C
SEMA3E
SPON1
ERG
SYT6
ITGA8
NR4A2
L2_CUX2_GULP1
L2_CUX2_MEPE
L3_CUX2_CD53
L4_RORB_ARHGAP24
L4_RORB_KCNH8_ABCA12
L4_RORB_KCNH8_ARHGAP24
L4_RORB_KCNH8_KCNB2
L4_RORB_KCNH8_PARD3
L4_RORB_KCNH8_SEMA5A
L4_RORB_KCNH8_SPOCK3
L4_RORB_MET_CRISPLD1
L4_RORB_MET_KCNIP1
L4_RORB_SV2C
L5_FEZF2_PDYN_TAFA1
L5_FEZF2_PDYN_THEMIS
L5_FEZF2_PDYN_TLL1
L5_FEZF2_TLE4_HTR2C
L5_RORB_SEMA3E
L5_RORB_SPON1
L6_FEZF2_TLE4_ERG
L6_FEZF2_TLE4_SYT6
L6_THEMIS_ITGA8
L6_THEMIS_NR4A2
E
ID2
LAMP5
NMBR
NOS1
PBX3
NCKAP5
PAX6
PVALB
FSTL5
SLIT2
COL5A2
CORIN
GLRA3
HPSE
SST
ALCAM
CALB1
RELN
VIP
CXCL14
SGCZ
TTN
UNC5D
GRM1
ARHGAP18
SEMA3E
TAC3
VWDE
log2 fold-change
5
4
3
2
1
0
ID2_LAMP5_NMBR
ID2_LAMP5_NOS1
ID2_LAMP5_PBX3
ID2_NCKAP5
ID2_PAX6
PVALB_FSTL5
PVALB_SLIT2_COL5A2
PVALB_SLIT2_CORIN
PVALB_SLIT2_GLRA3
PVALB_SLIT2_HPSE
SST_ALCAM
SST_CALB1
SST_NOS1
SST_RELN
SST_SLIT2
VIP_CXCL14_SGCZ
VIP_CXCL14_TTN
VIP_CXCL14_UNC5D
VIP_GRM1_ARHGAP18
VIP_GRM1_SEMA3E
VIP_GRM1_TAC3
VIP_GRM1_TTN
VIP_GRM1_VWDE

Fig. 2 Experimental procedure and snRNA-seq dataset
(A) Experimental design of the snRNA-seq measurement: tissue blocks from cortical areas V1 and V4 were dissected from sagittal slices of rhesus macaque brain, tissue was homogenized, nuclei purified using gradient centrifugation and neuronal nuclei were stained using NeuN with following FANS. Neuronal nuclei were sequenced using 10x Genomics assays. **(B)** Major neuronal families and their subtypes were detected using single nuclei RNA sequencing. UMAP representation of single nuclei transcriptomes is shown; nuclei are colored by their subtype. **(C)** UMAP representation of single nuclei, coloured by cortical area V1 and V4. **(D)** Heat map depicting expression of markers for principal neuronal subtypes, log2 fold-change is plotted. **(E)** Heat map depicting expression of markers for inhibitory neuronal subtypes, log2 fold-change is plotted.

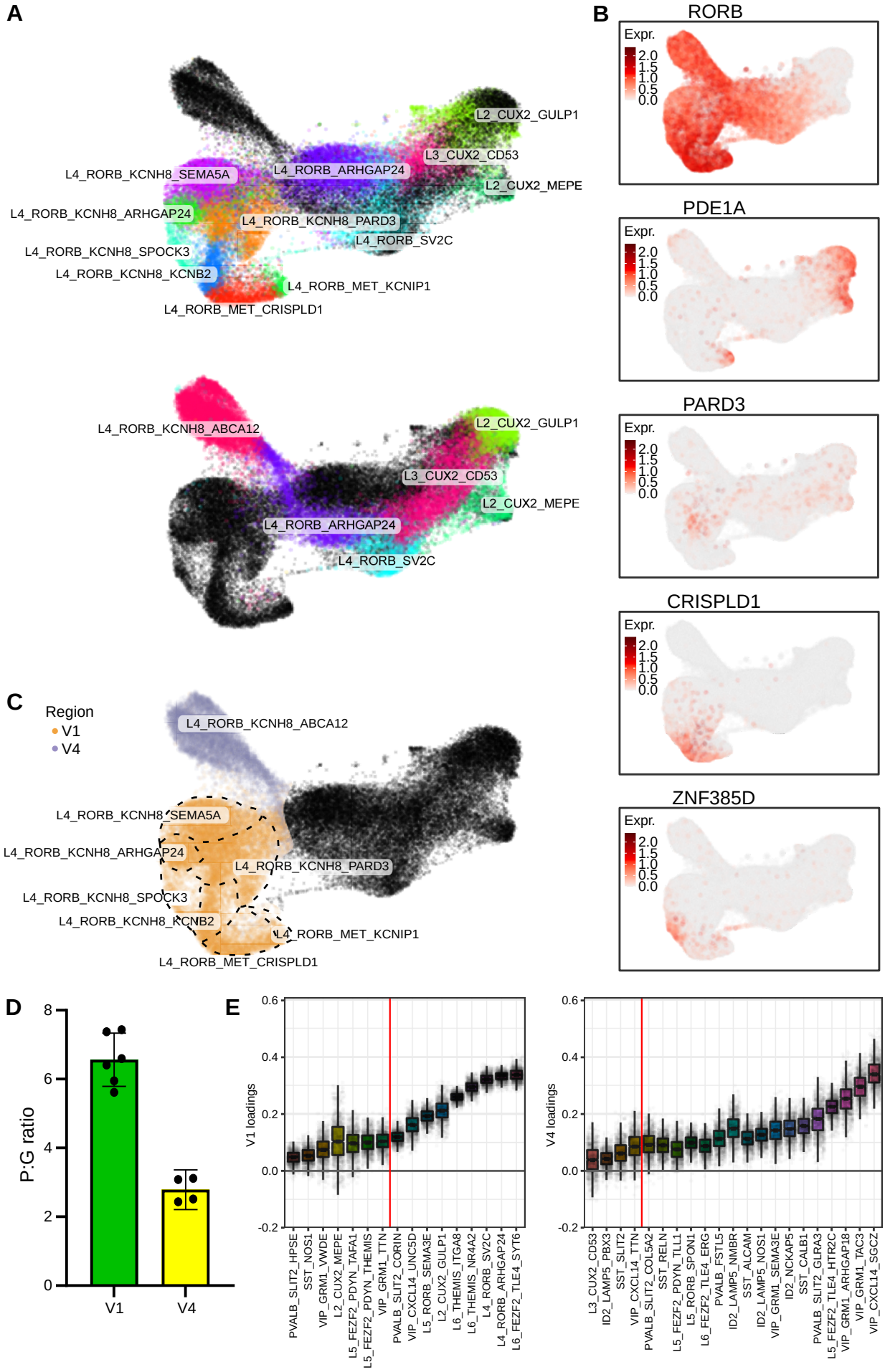
A
L2_CUX2_GULP1
L3_CUX2_CD53
L4_RORB_KCNH8_SEMA5A
L4_RORB_ARHGAP24
L2_CUX2_MEPE
L4_RORB_KCNH8_ARHGAP24
L4_RORB_KCNH8_PARD3
L4_RORB_SV2C
L4_RORB_KCNH8_SPOCK3
L4_RORB_KCNH8_KCNB2
L4_RORB_MET_KCNIP1
L4_RORB_MET_CRISPLD1
L4_RORB_KCNH8_ABCA12
L2_CUX2_GULP1
L3_CUX2_CD53
L2_CUX2_MEPE
L4_RORB_ARHGAP24
L4_RORB_SV2C
B
RORB
PDE1A
PARD3
CRISPLD1
ZNF385D
Expr.
2.0
1.5
1.0
0.5
0.0
C
Region
V1
V4
L4_RORB_KCNH8_ABCA12
L4_RORB_KCNH8_SEMA5A
L4_RORB_KCNH8_ARHGAP24
L4_RORB_KCNH8_PARD3
L4_RORB_KCNH8_SPOCK3
L4_RORB_KCNH8_KCNB2
L4_RORB_MET_KCNIP1
L4_RORB_MET_CRISPLD1
D
P:G ratio
0
2
4
6
8
V1
V4
E
V1 loadings
0.6
0.4
0.2
0.0
-0.2
PVALB_SLIT2_HPSE
SST_NOS1
VIP_GRM1_VWDE
L2_CUX2_MEPE
L5_FEZF2_PDYN_TAFA1
L5_FEZF2_PDYN_THEMIS
VIP_GRM1_TTN
PVALB_SLIT2_CORIN
VIP_CXCL14_UNC5D
L5_RORB_SEMA3E
L2_CUX2_GULP1
L6_THEMIS_ITGA8
L6_THEMIS_NR4A2
L4_RORB_SV2C
L4_RORB_ARHGAP24
L6_FEZF2_TLE4_SYT6
V4 loadings
0.6
0.4
0.2
0.0
-0.2
L3_CUX2_CD53
ID2_LAMP5_PBX3
SST_SLIT2
VIP_CXCL14_TTN
PVALB_SLIT2_COL5A2
SST_RELN
L5_FEZF2_PDYN_TLL1
L5_RORB_SPON1
L6_FEZF2_TLE4_ERG
PVALB_FSTL5
ID2_LAMP5_NMBR
SST_ALCAM
ID2_LAMP5_NOS1
VIP_GRM1_SEMA3E
ID2_NCKAP5
SST_CALB1
PVALB_SLIT2_GLRA3
L5_FEZF2_TLE4_HTR2C
VIP_GRM1_ARHGAP18
VIP_GRM1_TAC3
VIP_CXCL14_SGCZ

Fig. 3 Compositional differences in cell types within visual areas
(A) Top plot: V1 layer 4 neuronal subtypes (in color) segregate from V4 subtypes (in grey) mostly by the presence of layer 4 V1-specific neuronal subtypes of L4_RORB family (L4_RORB_KCNH8_SEMA5A, L4_RORB_KCNH8_ARHGAP24, L4_RORB_KCNH8_KCNB2, L4_RORB_KCNH8_PARD3, L4_RORB_KCNH8_SPOCK3, L4_RORB_MET_CRISPLD1, L4_RORB_MET_KCNIP1); Bottom plot: Similarly, V4 layer 4 subtypes (in color) segregate from V1 layer 4 subtypes (in grey) mostly by the presence of V4-specific subtype L4_RORB_KCNH8_ABCA12. UMAP representation of nuclei transcriptomes is shown. **(B)** Expression of marker genes being selected for further smFISH analysis based on their expression in cell clusters uniquely present in V1 layer 4. **(C)** V1 neuronal subtypes (orange) segregate from V4 subtypes (purple) in layer 4. **(D)** Relative number of principal to neurons to GABAergic neurons (P:G ratio) in areas V1 and V4. Bar indicated the mean and 95% CI across samples. **(E)** Further change in neuronal composition between V1 and V4 evaluated by compositional data analysis. Cell types distinguishing composition of V1 and V4 samples and present in both regions are shown, region-specific subtypes mentioned above were omitted. The y-axis indicates the separating coefficient for each cell type, with values corresponding to neurons with increased abundance in V1 (top) and V4 (bottom). The boxplots and individual data points show uncertainty based on bootstrap resampling of samples and cells. Red line represents cut-off for significance of adjusted (by the Benjamini-Hochberg method) P values (significant cell types are above the line).

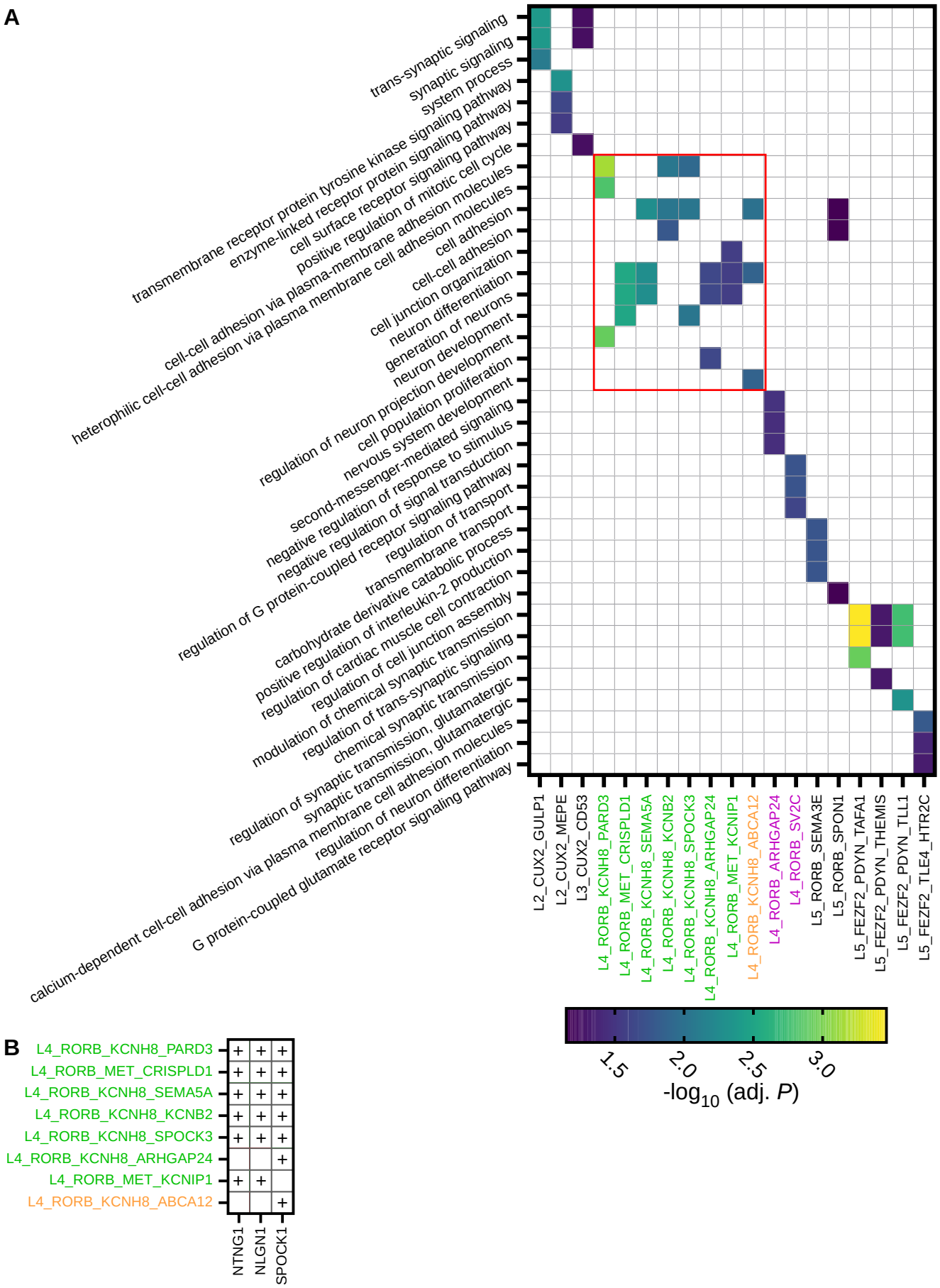
A
trans-synaptic signaling
synaptic signaling
system process
transmembrane receptor protein tyrosine kinase signaling pathway
enzyme-linked receptor protein signaling pathway
cell surface receptor signaling pathway
positive regulation of mitotic cell cycle
cell-cell adhesion via plasma-membrane adhesion molecules
heterophilic cell-cell adhesion via plasma membrane cell adhesion molecules
cell adhesion
cell-cell adhesion
cell junction organization
neuron differentiation
generation of neurons
neuron development
regulation of neuron projection development
cell population proliferation
nervous system development
second-messenger-mediated signaling
negative regulation of response to stimulus
negative regulation of signal transduction
regulation of G protein-coupled receptor signaling pathway
regulation of transport
transmembrane transport
carbohydrate derivative catabolic process
positive regulation of interleukin-2 production
regulation of cardiac muscle cell contraction
regulation of cell junction assembly
regulation of chemical synaptic transmission
modulation of chemical synaptic signaling
regulation of trans-synaptic signaling
chemical synaptic transmission
regulation of synaptic transmission, glutamatergic
synaptic transmission, glutamatergic
calcium-dependent cell-cell adhesion via plasma membrane cell adhesion molecules
regulation of neuron differentiation
G protein-coupled glutamate receptor signaling pathway
L2_CUX2_GULP1
L2_CUX2_MEPE
L3_CUX2_CD53
L4_RORB_KCNH8_PARD3
L4_RORB_MET_CRISPLD1
L4_RORB_KCNH8_SEMA5A
L4_RORB_KCNH8_KCNB2
L4_RORB_KCNH8_SPOCK3
L4_RORB_KCNH8_ARHGAP24
L4_RORB_MET_KCNIP1
L4_RORB_KCNH8_ABCA12
L4_RORB_ARHGAP24
L4_RORB_SV2C
L5_RORB_SEMA3E
L5_RORB_SPON1
L5_FEZF2_PDYN_TAFA1
L5_FEZF2_PDYN_THEMIS
L5_FEZF2_PDYN_TLL1
L5_FEZF2_TLE4_HTR2C
1.5
2.0
2.5
3.0
-log10 (adj. P)
B
L4_RORB_KCNH8_PARD3
L4_RORB_MET_CRISPLD1
L4_RORB_KCNH8_SEMA5A
L4_RORB_KCNH8_KCNB2
L4_RORB_KCNH8_SPOCK3
L4_RORB_KCNH8_ARHGAP24
L4_RORB_MET_KCNIP1
L4_RORB_KCNH8_ABCA12
NTNG1
NLGN1
SPOCK1

Fig. 4 Enriched GO terms show similarities between unique V1 and V4 subtypes
(A) Heat map of top 3 enriched GO terms per indicated cell type from a list of enriched GO terms of upregulated genes is shown. GO terms are shown by adjusted p-value. Cell types unique in V1 are colored in green, cell type unique for V4 in orange and layer 4 cell types present in V1 and V4 in purple. **(B)** Genes associated with the top 3 enriched GO terms for the cell types uniquely found in V1 (green) and V4 (orange).

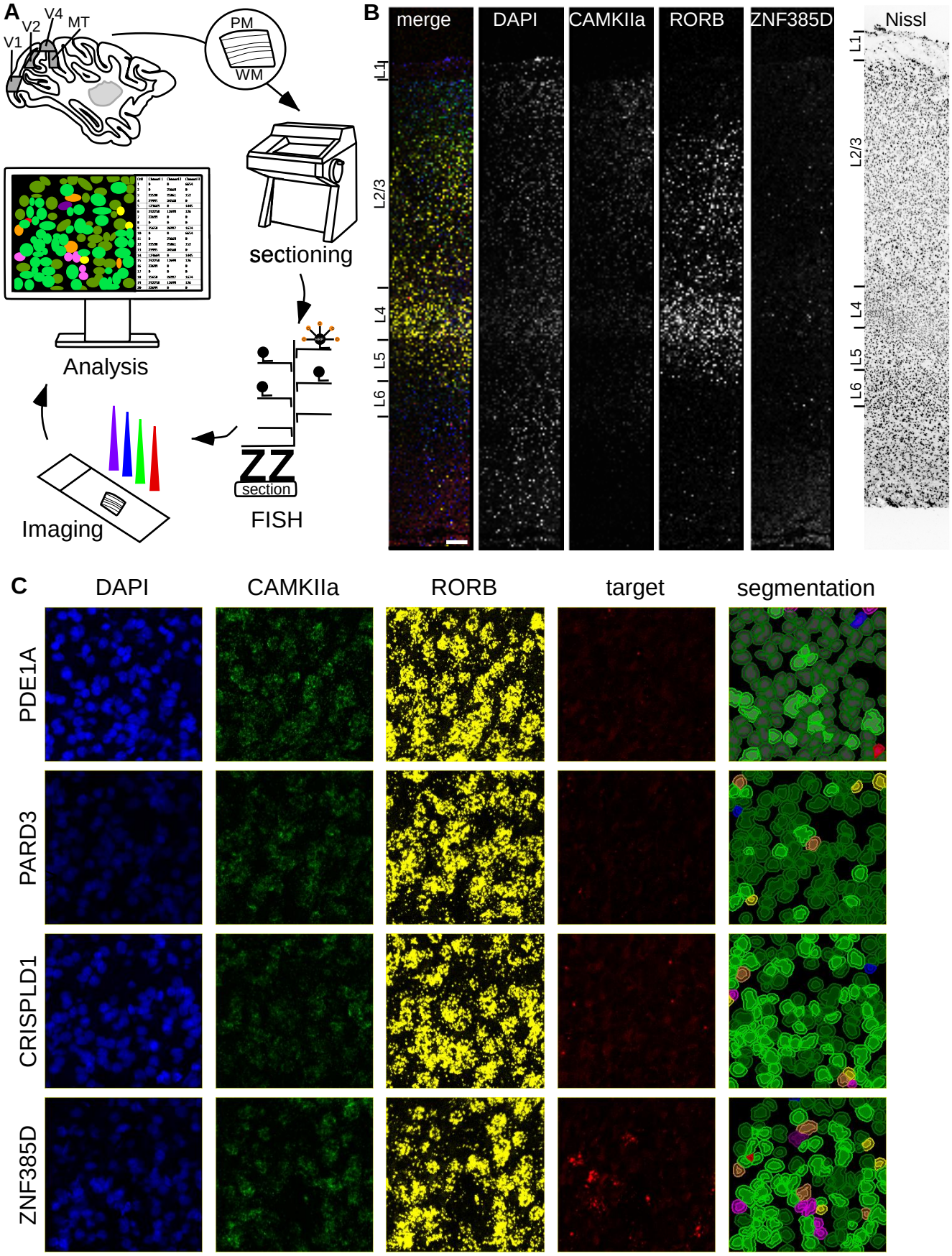
A
V1
V2
V4
MT
PM
WM
sectioning
Analysis
FISH
section
Imaging
B
merge
DAPI
CAMKIIa
RORB
ZNF385D
Nissl
L1
L2/3
L4
L5
L6
C
DAPI
CAMKIIa
RORB
target
segmentation
PDE1A
PARD3
CRISPLD1
ZNF385D

Fig. 5 Experimental design for quantitative smFISH
(A) Experimental design of the fluorescent in situ hybridization workflow. Tissue blocks were extracted from sagittal brain slices, sectioned into 10 µm sections, conducted to the RNAscope Multiplex Fluorescent V2 Assay, visualized utilizing a Leica SP8 confocal microscope and analyzed using the QuPath software. **(B)** Overview image showing an exemplary staining. Laminar patters for *CAMK2A*, *RORB*, the respective target and Nissl from the pia mater to the white matter. Fluorescent imaged from fourfold stain 10 µm thick section from V1. Scale bar 200µm. Brightfield image from 10µm section from V1. Scale bar 200µm **(C)** Exemplary single color images from layer 4 in V1. DAPI nucleus staining: blue; *CAMK2A* hybridization: green; *RORB* hybridization: yellow and target hybridization: red. Segmentation: pink: negative; red: target +; blue: *CAMK2A*+; yellow: *RORB*+; dark green: *CAMK2A*+ *RORB*+; orange: *RORB*+ target+; purple: *CAMK2A*+ target+; light green: *CAMK2A*+ *RORB*+ target+. Scale bar 45 µm.

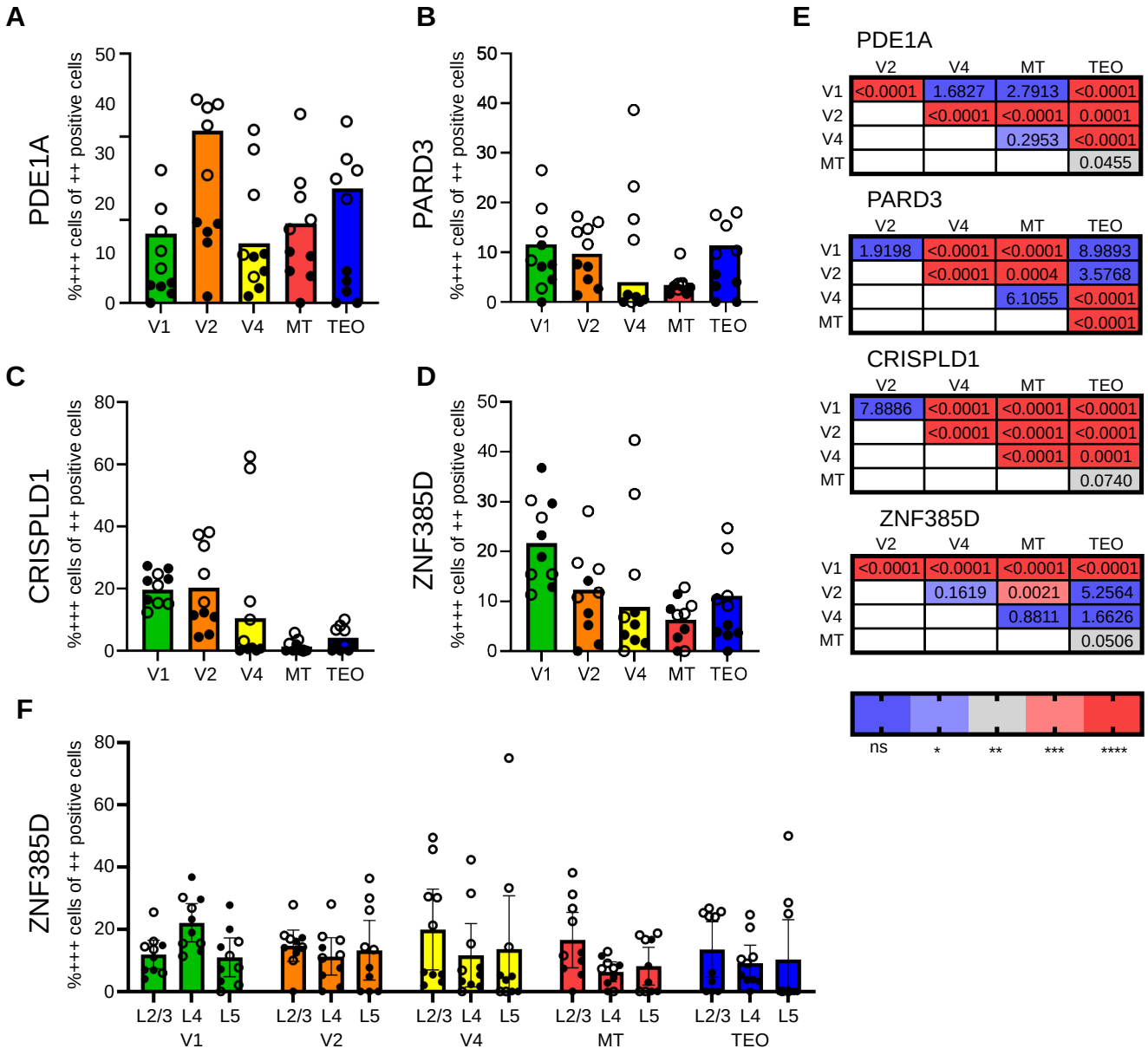

Fig. 6 Quantification of smFISH reveals gradient along dorsal stream
(A-D) Percentage of CamKIIa+ RORB+ target+ cells of CamKIIa+ RORB+ cells in layer 4 over V1, V2, V4, MT, and TEO. Symbols represent data from 10 counting windows over n = 2 rhesus macaques, circles represent monkey E and dots represent monkey S, bar represent means, error bars represent 95% CIs. **(E)** Significance (single cells chi-square tested, Bonferroni corrected). **(F)** Percentage of *CAMK2A*+ *RORB*+ target+ cells of *CAMK2A*+ *RORB*+ cells over layer 2/3, layer 4 and layer 5 for V1, V2, V4, MT and TEO. Symbols represent data from 10 counting windows over n = 2 rhesus macaques, circles represent monkey E and dots represent monkey S, bar represent means, error bars represent 95% CIs.